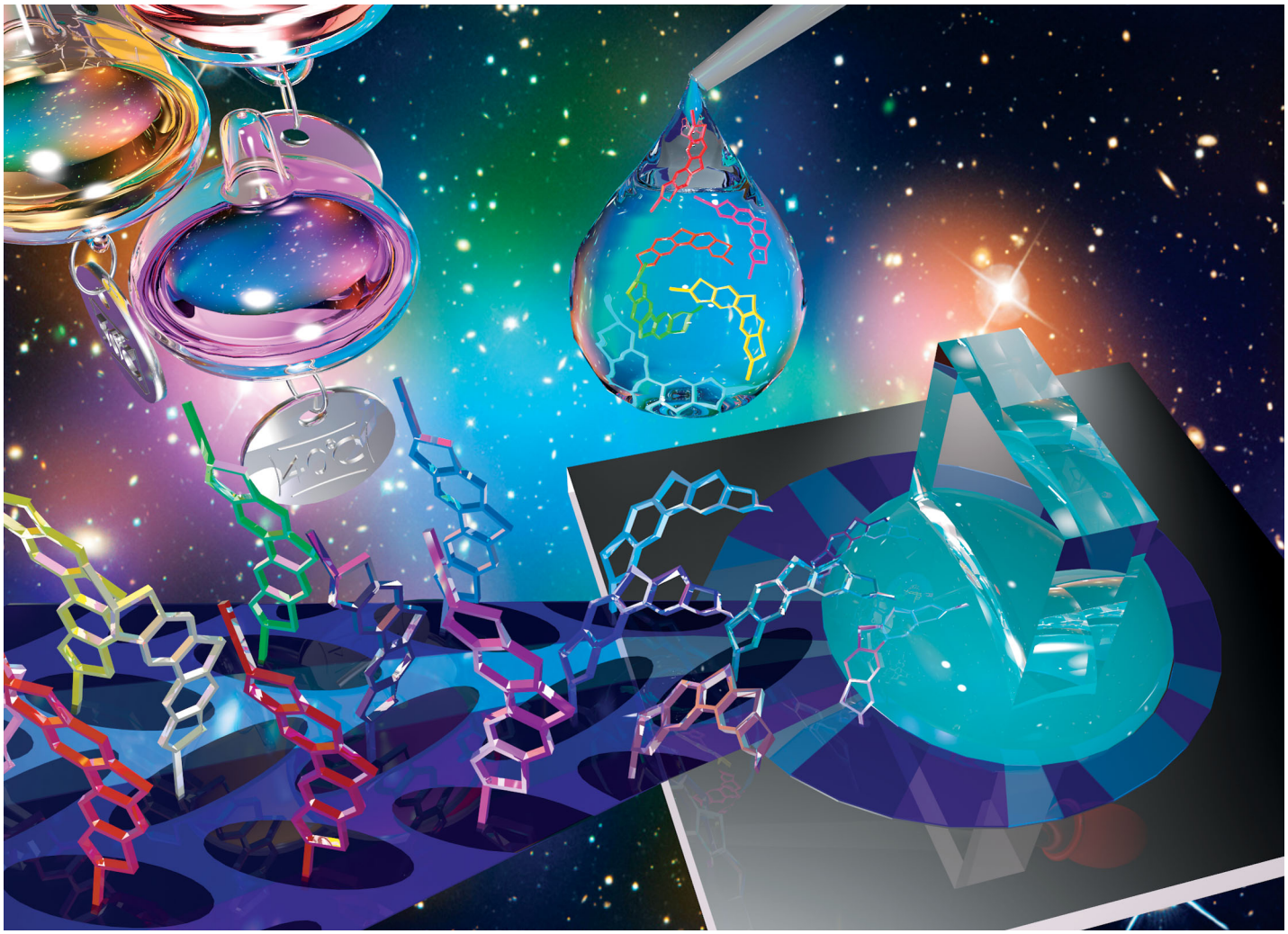

Showcasing research from the Department of Advanced Materials Science, Graduate School of Frontier Sciences, The University of Tokyo.

High performance solution-crystallized thin-film transistors based on V-shaped thieno[3,2-*f*:4,5-*f*′]bis[1]benzothiophene semiconductors

Solution-processable V-shaped thieno[3,2-*f*:4,5-*f*′]-bis[1]benzothiophene (**TBBT-V**) semiconductors were developed by a modular synthetic approach. Decyl-substituted **TBBT-V** easily formed single-crystalline thin-films by an edge-casting method, exhibiting remarkable hole mobility up to 6.2 $cm^2\ V^{-1}\ s^{-1}$ in a field-effect transistor.

As featured in:

See Toshihiro Okamoto *et al.*, *J. Mater. Chem. C*, 2017, **5**, 1903.

ROYAL SOCIETY OF CHEMISTRY

rsc.li/materials-c

Registered charity number: 207890

Journal of Materials Chemistry C

PAPER

View Article Online
View Journal | View Issue

Cite this: J. Mater. Chem. C, 2017, 5, 1903

High performance solution-crystallized thin-film transistors based on V-shaped thieno[3,2-*f*:4,5-*f*′]-bis[1]benzothiophene semiconductors†

Chikahiko Mitsui,[a] Hiroaki Tsuyama,[b] Ryoji Shikata,[c] Yoshinori Murata,[c] Hiroyuki Kuniyasu,[a] Masakazu Yamagishi,[d] Hiroyuki Ishii,[e] Akito Yamamoto,[a] Yuri Hirose,[f] Masafumi Yano,[c] Tsunayoshi Takehara,[g] Takeyuki Suzuki,[g] Hiroyasu Sato,[h] Akihito Yamano,[h] Eiji Fukuzaki,[b] Tetsuya Watanabe,[b] Yoshihisa Usami,[b] Jun Takeya[af] and Toshihiro Okamoto*[ai]

Received 1st November 2016,
Accepted 20th January 2017

DOI: 10.1039/c6tc04721a

rsc.li/materials-c

A new class of solution-processable thieno[3,2-*f*:4,5-*f*′]bis[1]benzothiophene (**TBBT-V**) semiconductors are investigated. Semiconductors with decyl substituents and two kinds of π-extended decylthienyl substituents are facially derivatized from functionalized dibromo-substituted **TBBT-V** *via* either a Negishi or a Stille cross coupling procedure. The solubilities of **TBBT-V** semiconductors are somewhat higher than those of their previously developed dinaphtho[2,3-*b*:2′,3′-*d*]thiophene (**DNT-V**) counterparts. Single crystal analysis together with a calculation study on the transfer integral and the band structure in decyl-substituted **TBBT-V** (**C_{10}-TBBT-V**) clarifies that these semiconductors form two-dimensionally ordered herringbone packing structures and the effective mass in the columnar direction rivals that of the previously developed decyl-substituted **DNT-V**. The carrier mobilities of **TBBT-V** derivatives in solution grown into single-crystalline films are remarkable (up to 6.2 $cm^2\ V^{-1}\ s^{-1}$). Furthermore, their operation voltages are apparently lower than those of previously developed **DNT-V** derivatives due to the optimized ionization potential of the **TBBT-V** core and further π-extension by substitution of the thienyl groups.

Introduction

Powered by organic syntheses, structural and electronic modifications of organic molecules represent desired functionalities in the field of materials science. Recently, functionalized organic π-conjugated materials have expanded the potential of plastic electronics, and have received great interest as next-generation printable and flexible electronic devices.[1,2] Among the π-conjugated organic materials developed to date, linearly benzene/heterole fused molecules have been extensively studied as organic field-effect transistors (OFETs).[3–5] Highly π-electron conjugated pentacene[6] and dinaphtho[2,3-*b*:2′,3′-*f*]thieno[3,2-*b*]-thiophene (**DNTT**)[7] are regarded as the benchmark due to their excellent semiconducting behavior compared to that of amorphous silicon (carrier mobility: ∼1 $cm^2\ V^{-1}\ s^{-1}$).

However, thin films are fabricated by the vacuum deposition method because solution processing is problematic due to their poor solubilities. The fatal drawbacks of **DNTT** have been overcome by structural modifications; for example, the introduction of long alkyl chains (**C_{10}-DNTT**) as well as the replacement of the smaller π-conjugated core of [1]benzothieno[3,2-*b*][1]benzothiophene with long alkyl chains (**C_8-BTBT**) have realized solution-processable organic semiconductors with high carrier mobilities, which exceed 10 $cm^2\ V^{-1}\ s^{-1}$.[8–10] Recently, we reported that conceptually new V-shaped π-conjugated molecules, dinaphtho[2,3-*b*:2′,3′-*d*]thiophene (**DNT-V**) and alkylated derivatives, are promising candidates for solution-processable organic semiconductors.[11]

Due to the presence of an internal dipole moment (1.10 debye calculated at the B3LYP/6-31G* level) in the **DNT-V** core, **DNT-V**

[a] Department of Advanced Materials Science, Graduate School of Frontier Sciences, The Univ. of Tokyo, 5-1-5 Kashiwanoha, Kashiwa, Chiba 277-8561, Japan. E-mail: tokamoto@k.u-tokyo.ac.jp
[b] Fuji Film Corp., 577 Ushijima, Kaisei-machi, Ashigarakami-gun, Kanagawa 258-8577, Japan
[c] Graduate School of Science and Engineering, Kansai Univ., 3-3-35 Yamate-cho, Suita, Osaka 564-8680, Japan
[d] National Institute of Technology, Toyama College, 13 Hongo-machi, Toyama, Toyama 939-8630, Japan
[e] Division of Applied Physics, Faculty of Pure and Applied Sciences, University of Tsukuba, 1-1-1 Tennodai, Tsukuba, Ibaraki 305-8573, Japan
[f] PI-Crystal Inc., 2-7-38 Nishimiyahara, Yodogawa, Osaka 532-0004, Japan
[g] Comprehensive Analysis Center (CAC), The Institute of Scientific and Industrial Research (ISIR), Osaka Univ., 8-1 Mihogaoka, Ibaraki, Osaka 567-0047, Japan
[h] Rigaku Corp., 3-9-12 Matsubara-cho, Akishima, Tokyo 196-8666, Japan
[i] PRESTO, JST, 4-1-8 Honcho, Kawaguchi, Saitama, 332-0012, Japan

† Electronic supplementary information (ESI) available. CCDC 1503965. For ESI and crystallographic data in CIF or other electronic format see DOI: 10.1039/c6tc04721a

itself exhibits a good solubility of over 0.1 wt% at room temperature in common organic solvents, whereas pentacene and **DNTT** have two-orders of magnitude lower solubilities under the same conditions. Furthermore, alkylated **DNT-V** derivatives exhibit one order of magnitude higher solubility than the parent **DNT-V**, realizing solubilities exceeding 1.0 wt%, which means that alkylated **DNT-V**s should be applicable to commonly used solution-processing techniques. However, one drawback of the **DNT-V** core is that the HOMO energy level of **DNT-V** (−5.41 eV) is somewhat high compared to those of pentacene (−4.60 eV) and **DNTT** (−5.18 eV) due to the shorter π-conjugation length (estimated by the theoretical calculations). This results in the large voltage operation in OFETs.[11] Therefore, further π-electron conjugation of the π-core is demanded. Additionally, from the viewpoint of synthetic methodology, selective and direct functionalization on the outer benzene ring of the **DNT-V** core is not straightforward due to the poor regioselectivity of the parent **DNT-V**.

In this work, we focus on thieno[3,2-*f*:4,5-*f*′]bis[1]benzothiophene (hereinafter denoted **TBBT-V**), where two thiophene rings replace the outer benzene rings of the **DNT-V** core. Thus, **TBBT-V** is a platform for selective functionalization at the α-position of the outer thiophene ring. As described in Fig. 1, a density functional theory (DFT) calculation study suggests that **TBBT-V** exhibits a similar orbital distribution in the highest occupied molecular orbital (HOMO) to that of **DNT-V**. The calculated HOMO energy level of **TBBT-V** (−5.46 eV) is almost the same as that of **DNT-V** (−5.41 eV). Taking into account the injection barrier from commonly used gold electrodes (Fermi level: −5.1 to −4.9 eV), this trend is beneficial for designing p-type materials for low threshold voltage applications. Furthermore, **TBBT-V** and its derivatives are assumed to have a sufficient solubility for printing processes due to the internal dipole moment (2.26 debye).

Although the **TBBT-V** core and its device performance in vacuum deposited thin-film transistors have been reported by Neckers *et al.*,[12,13] the series of **TBBT-V** derivatives is yet to be studied, especially the aggregated structures and the carrier-transporting properties. Herein we demonstrate that alkylated **TBBT-V** with decyl groups (**C_{10}-TBBT-V**) and π-extended thienyl-substituted **TBBT-V** molecules with decyl groups at the alpha and beta positions of the thienyl groups (**α-C_{10}-Th-TBBT-V** and **β-C_{10}-Th-TBBT-V**) have potential as a new class of organic semiconductors (Fig. 1). **α-C_{10}-Th-TBBT-V** and **β-C_{10}-Th-TBBT-V** should have higher HOMO levels (Fig. S1, ESI†).

Starting from the functionalized **TBBT-V**, which is brominated at the α positions of the outer thiophene rings, all **TBBT-V** derivatives are easily synthesized *via* a coupling reaction. The solubilities of **TBBT-V** and **C_{10}-TBBT-V** are somewhat higher than those of their **DNT-V** counterparts, while those of the π-extended **Th-TBBT-V** derivatives are two-orders of magnitude lower even at elevated temperatures. In terms of the ionization potentials, **TBBT-V** itself exhibits a smaller value (5.61 eV) compared to **DNT-V** (5.72 eV). Furthermore, those of **C_{10}-TBBT-V** and **C_{10}-Th-TBBT-V**s range from 5.01–5.26 eV. Single crystal analysis reveals that **C_{10}-TBBT-V** aggregates into two-dimensional typical herringbone packing structures. Finally, the charge transporting properties of **TBBT-V** derivatives evaluated on transistors using solution-crystallized single-crystalline thin-films result in a high carrier mobility of up to 6.2 $cm^2 V^{-1} s^{-1}$ with an apparently lower voltage in p-type operations than in the **DNT-V** cases. As expected, π-extended **β-C_{10}-Th-TBBT-V** exhibits a much lower or negligible threshold voltage due to the smaller ionization potential.

Results and discussion

Synthesis

Scheme 1 illustrates the synthetic route for the **TBBT-V** derivatives. The **TBBT-V** core was synthesized according to the literature.[12] By treatment of **TBBT-V** with lithium 2,2,6,6-tetramethylpiperidide (LiTMP) as a base, the α positions of the outer thiophene rings were selectively deprotonated and subsequent bromination by 1,2-dibromo-1,1,2,2-tetrachloroethane afforded **Br-TBBT-V** as a platform for facile functionalization. Alkylation and arylation reactions were easily carried out *via* palladium-catalyzed cross

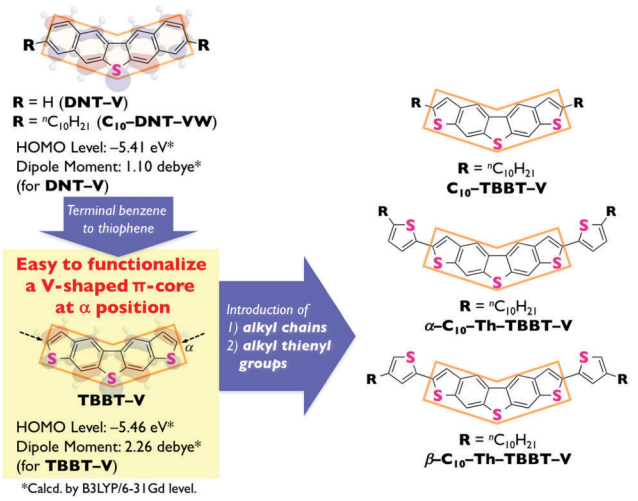

Fig. 1 Chemical structures and DFT calculations of TBBT–V and its derivatives. DNT–V and its derivatives are shown for comparison.

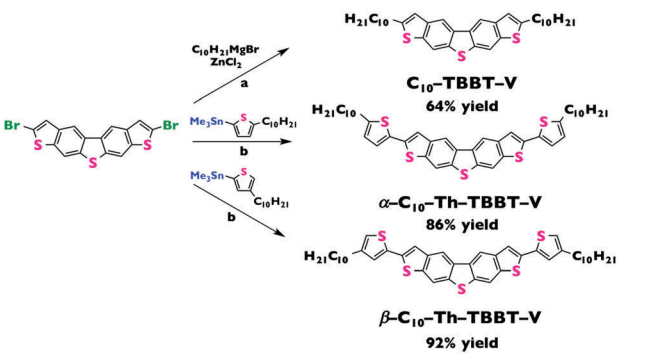

Scheme 1 Reaction conditions: (a) $^nC_{10}H_{21}MgBr$ (4.0 mol amt.), $ZnCl_2$ (4.0 mol amt.), $PdCl_2(dppf)\cdot CH_2Cl_2$, PhMe (0.1 M), 70 °C, 18 h and (b) trimethylstannyl derivatives (2.6 mol amt.), $Pd(PPh_3)_4$ (5 mol%), LiCl (2.6 mol amt.), DMF (0.1 M), 100 °C, 10 h.

Table 1 Solubilities and IP of **TBBT-V** and **DNT-V** derivatives

Compounds	Solubility (wt%)			IP (eV)
	$CHCl_3$	Toluene	1,2-Dichlorobenzene	
TBBT-V	0.17	0.15	0.25	5.61
C_{10}-TBBT-V	1.1	0.54	0.99	5.26
α-C_{10}-Th-TBBT-V	0.017[a]	0.019[a]	0.016[a]	5.10
β-C_{10}-Th-TBBT-V	0.093[a]	0.065[a]	0.055[a]	5.01
DNT-V	0.18	0.17	0.25	5.72
C_{10}-DNT-VW	0.47	0.38	0.47	5.45

[a] Solubility at 60 °C.

coupling in moderate yields of 64–92%, while hexyl and dodecyl-substituted **TBBT-V** reported previously were synthesized from the corresponding alkylated thiophenes as starting materials in the initial step.[14]

Solubility tests

To evaluate solution processability, solubility tests of the synthesized **TBBT-V** derivatives were conducted at room temperature for all derivatives and at 60 °C for π-extended derivatives (Table 1). At first, the solubility of the parent **TBBT-V** core was compared with that of **DNT-V**. **TBBT-V** exhibits a similar solubility to **DNT-V** in several types of solvents. As reported previously, the solubility of alkyl substituted **DNT-V** is more than double that of **DNT-V** itself, allowing us to apply solution processing at low temperatures.[11] In the case of the **TBBT-V** core, **C_{10}-TBBT-V** also exhibits an improved solubility up to 1.1 wt%. In contrast, introduction of the thienyl rings between the core and the alkyl chain decreases the solubility due to the extension of the π-electron system. Thus, **α-** and **β-C_{10}-Th-TBBT-V** exhibit a solubility less than 0.01 wt% at room temperature and in the range of 0.017–0.093 wt% at 60 °C, respectively. The results indicate that several solution processes can be applied to **C_{10}-TBBT-V**, although the relatively low solubilities of **α-** and **β-C_{10}-Th-TBBT-V** prompted us to evaluate single-crystalline thin films grown by the edge-casting method[15] at an elevated temperature on a hot plate.

Ionization potentials

As summarized in Table 1, the photoelectron yield spectroscopy (PYS) measurements reveal that **TBBT-V** itself possesses a smaller ionization potential (IP) (5.61 eV) than **DNT-V** (5.72 eV). **C_{10}-TBBT-V** exhibits an IP as small as 5.26 eV. Thienyl embedded **α-** and **β-C_{10}-Th-TBBT-V** have even smaller values of 5.10 and 5.01 eV, respectively, due to a combination of electron donation by the alkyl chain and effective π-electron conjugation by the thienyl moieties (Fig. S2, ESI†). The IP values of **TBBT-V** derivatives are almost consistent with the trend obtained from the theoretical calculations (Fig. 1 and Fig. S1, ESI†).

Regarding **α-C_{10}-Th-TBBT-V** and **β-C_{10}-Th-TBBT-V**, a high chemical stability is ascertained by measuring the time-dependent UV-vis absorption spectrum in solution under air. No spectral change is observed around two weeks (Fig. S3 and S4, ESI†). Thus, **TBBT-V** derivatives are chemically stable under ambient conditions because the **TBBT-V** core is an isoelectronic structure with pentaphene. **TBBT-V** potentially shows a lower ionization potential and a higher chemical stability than pentacene, which is active toward photo-oxidation. Their optimized ionization potentials in the range of 5.01–5.26 eV afford their chemical stabilities toward photo-oxidation under ambient conditions. Thus, all of the synthesized **TBBT-V** derivatives are air-stable organic semiconductors.

Crystallography and theoretical calculations

To unveil the molecular and packing structure as well as to calculate the electronic band structure in the aggregated form, we carried out X-ray single crystal analysis. The single crystals of **C_{10}-TBBT-V**, **α-**, and **β-C_{10}-Th-TBBT-V** were grown by solution techniques involving two-layer diffusion between good and poor solvents to obtain platelet single crystals for all compounds. Among them, X-ray single crystal analyses were successfully performed on only **C_{10}-TBBT-V**. The laboratory X-ray instruments could not collect satisfactory data for **α-** and **β-C_{10}-Th-TBBT-V**, which may be attributed to the low quality of their single crystals, the intrinsic molecular disordering at the rotations between the thienyl and the core units, and the large cell size judging from their low symmetries.

The prominent central sulfur atom interacts with the adjacent molecules by C–H···π interactions, so that the **TBBT-V** core geometry deforms into the bent conformation. Its bent angle between the inner benzene rings is 11.27° (Fig. 2b), which is similar to the previously reported **C_{10}-DNT-VW** (12.42°) (Fig. S9, ESI†).[11] To simplify the following arguments, we define the head (H) and the tail (T) of the **TBBT-V** core; the H part corresponds to the side of the prominent sulfur atom of the core structure and the T part is the opposite side of the molecule (Fig. 2a). **C_{10}-TBBT-V** forms a two-dimensionally ordered herringbone packing structure (Fig. 3b). In this herringbone packing structure, **C_{10}-TBBT-V** possesses two types of short contacts (Fig. 3a). In H-to-H molecules, short contacts by S···π interactions (S1···C2: 3.359 Å and S1···C3: 3.332 Å), which are defined as values smaller than the sum of van der Waals radii for carbon (1.70 Å) and sulfur (1.85 Å),[16] are observed between the central thiophene rings. On the other hand, in T-to-T molecules, short

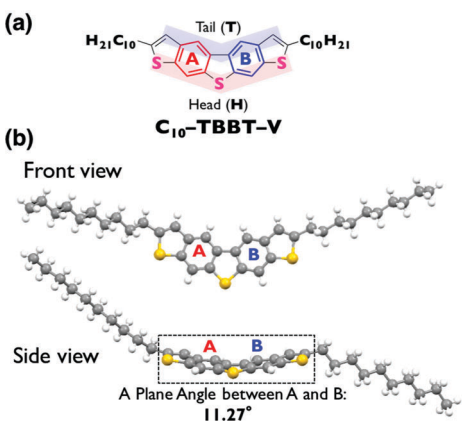

Fig. 2 (a) Chemical structure of **C_{10}-TBBT-V** and the definition of head (H) and tail (T). (b) Front and side views of the molecular structure of **C_{10}-TBBT-V**.

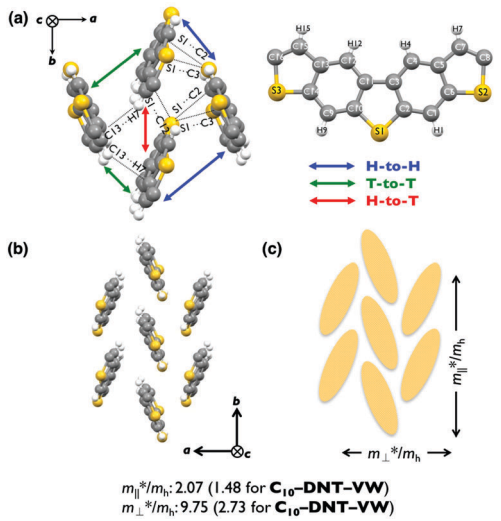

Fig. 3 (a) Packing structure of **C_{10}-TBBT-V** with short contacts (decyl groups are omitted for clarity). (b) Packing structure of **C_{10}-TBBT-V**. (c) Image of a typical herringbone packing structure together with the hole effective masses in the columnar direction ($m_{\parallel}$*) and the transverse direction ($m_{\perp}$*). (Decyl groups are omitted for clarity.)

contacts (C13···H7: 2.858 Å) are observed due to the C–H···π interactions between the inner benzene and the outer thiophene. Furthermore, in the H-to-T relationship, a slightly longer short contact due to the S···π interactions (S1···C12: 3.476 Å) is observed between the inner benzene and the inner thiophene. Although **C_{10}-TBBT-V** shows a slight molecular displacement of 0.35 and 0.64 Å, 0.23 Å, 1.01 and 1.33 Å for H-to-H, H-to-T, and T-to-T, respectively (Fig. S10a, ESI†), compared with **C_{10}-DNT-VW** of the layer-by-layer lamella structures without displacement in the molecular long axis direction (Fig. S10b, ESI†), such attractive herringbone-type packing arrangements with small displacements lead to effective carrier transport along with a higher solubility than **C_{10}-DNT-VW**.

Based on the packing structure, we estimated the intermolecular electronic couplings by the transfer integral (t) for holes using the dimer approach[17] at the PBEPBE/6-31G(d) level. The t values of **C_{10}-TBBT-V** are −67, 52, and −10 meV for t_{HH}, t_{HT}, and t_{TT}, respectively. In the case of **C_{10}-DNT-VW**, the energy levels of the HOMO and NHOMO are very close (Fig. S13, ESI†), but their calculated t values are −14, 18, and −32 meV for t_{HH}, t_{HT}, and t_{TT} (between HOMOs), and −61, 45, and −37 meV for t_{HH}, t_{HT}, and t_{TT} (between NHOMOs), respectively (Table 2 and Fig. S14, ESI†).

Table 2 Transfer integrals and effective masses of **TBBT-V** and **DNT-V** derivatives

	Transfer integral[a] (meV)			Effective mass	
Compounds	H–H	H–T	T–T	Column	Transverse
C_{10}-TBBT-V	−67[a]	52[a]	−10[a]	2.07	9.75
C_{10}-DNT-VW	−14[a]	18[a]	−32[a]	1.48	2.73
	−61[b]	45[b]	−37[a]		

[a] Transfer integrals between HOMOs. [b] Transfer integrals between NHOMOs.

We also calculated the electronic band structure to quantitatively analyze the carrier transporting ability at the same level as the intermolecular electronic couplings *via* the periodic boundary condition. The carrier mobility is inversely proportional to the effective mass as described by the following equation

$$\mu = q\tau_r/m^*$$

where μ: mobility, q: carrier charge, τ_r: relaxation time, and m^*: effective mass.[18]

Here, we formulate the effective masses in the columnar direction as $m_{\parallel}$* and in the transverse direction as $m_{\perp}$*. Fig. 3c summarizes the calculated effective hole masses for **C_{10}-TBBT-V** and **C_{10}-DNT-VW**. The mass of the columnar direction ($m_{\parallel}$*/m_h) for **C_{10}-TBBT-V** is slightly larger than that of **C_{10}-DNT-VW**. Clearly, $m_{\parallel}$*/m_h (2.07) is smaller than $m_{\perp}$*/m_h (9.75) (Table 2 and Fig. S15, ESI†), indicating that **C_{10}-TBBT-V** has a somewhat larger effective mass and less-balanced two-dimensional transport than **C_{10}-DNT-VW**. Furthermore, the columnar direction of **C_{10}-TBBT-V** is preferable for transport to the transverse direction.

Transistor performance

Next we studied the performance of the field-effect transistors using single-crystalline thin films of **TBBT-V** derivatives and compared the results with those of **C_{10}-DNT-VW**. Single-crystalline films were grown on the substrates by the edge-casting method.[15] Each crystalline film had a thickness of tens of nanometers. After removing the residual solvent by heating in a vacuum, F_4–TCNQ, which helps hole injection into the organic semiconductors, gold electrodes were successively deposited on top of the prepared single-crystalline thin film through a patterned shadow mask to construct the bottom-gate-top-contact structure (Fig. 4a and b).

To determine the direction of the crystals, we performed transmission X-ray diffraction measurements. The diffractions were measured using a Rigaku R-AXIS RAPID II imaging plate diffractometer with CuKα radiation. Fig. 4c and d show the obtained diffraction patterns. The Laue spots for the **C_{10}-TBBT-V** film can be attributed as described in the figure assuming that the crystalline film has the same structure as that obtained from the single crystal structure analysis. As shown in the in-plane diffraction pattern (Fig. 4c), the direction of the crystal growth, or the channel direction, is almost along the b-axis. (The b-axis agrees with the b*-axis because of the monoclinic structure with $\beta \neq 90°$.) Furthermore, the c*-axis should be almost perpendicular to the substrate (Fig. 4d). The results indicate that a favorable transporting channel can be constructed in the **C_{10}-TBBT-V** solution-crystallized film (Fig. 4e).

Furthermore, AFM images indicate that the surface of a **C_{10}-TBBT-V** crystalline film is molecularly flat (Fig. S17, ESI†). TFT performances were measured under ambient conditions. Table 3 summarizes the transistor parameters, including the maximum and average values of mobility, μ_{max} and μ_{ave}, threshold voltage, V_{th}, and current on/off ratio, I_{on}/I_{off}. All the compounds exhibit typical p-type behaviors with different threshold voltages, which reflect their ionization potentials. **C_{10}-TBBT-V** shows a

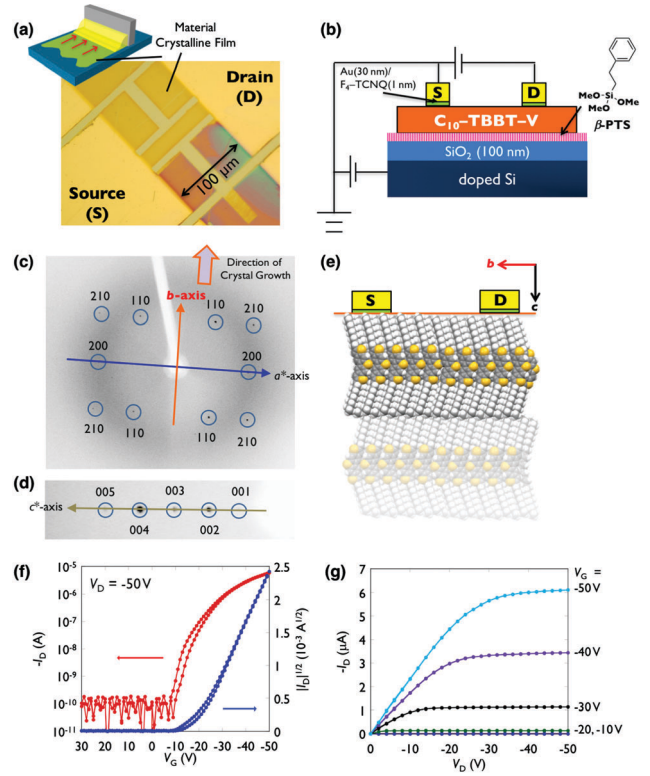

Fig. 4 (a) Optical microscope images of the **C_{10}-TBBT-V** crystalline thin film fabricated by the edge-casting method. (b) Device configuration of solution-processed transistors. (c) In-plane diffraction pattern and (d) out-of-plane diffraction pattern of the **C_{10}-TBBT-V** solution-crystallized film. (e) A molecular orientation of **C_{10}-TBBT-V** in solution-crystallized thin films. (f and g) Transfer and output characteristics of a **C_{10}-TBBT-V** based device (L = 100 μm, W = 21 μm after laser cut) fabricated on a β-PTS-treated SiO_2 substrate.

high carrier mobility up to 6.2 $cm^2\ V^{-1}\ s^{-1}$ along the columnar direction, as confirmed by the transmission X-ray diffraction measurements.

Considering that this molecule assumes a less-balanced two-dimensional transporting property as revealed by the band calculation, the obtained value from the single-crystal film is about three times higher than that of a polycrystalline thin film (1.8 $cm^2\ V^{-1}\ s^{-1}$) (see the ESI†). The carrier mobility of the **C_{10}-TBBT-V** single crystal is comparable to or slightly lower than those of the previously reported **C_{10}-DNT-VW** and **C_6-DNT-VW** (6.5 and 9.5 $cm^2\ V^{-1}\ s^{-1}$, respectively) because the effective mass of **C_{10}-TBBT-V** is larger and more isotropic than that of **C_{10}-DNT-VW**. However, it is noteworthy that, as expected, the threshold voltage of **C_{10}-TBBT-V**, −20 to −15 V, is lower than that of **C_{10}-DNT-VW** (V_{th} = −30 to −25 V, Fig. S21, ESI†) for the same device structure. Furthermore, the π-extended molecule, **β-C_{10}-Th-TBBT-V**, shows a much lower voltage operation (V_{th} = −10 to −5 V) with a carrier mobility as high as 2.3 $cm^2\ V^{-1}\ s^{-1}$ (Fig. S20, ESI†). Due to the small ionization potential of 5.01 eV, this device does not require the F_4–TCNQ, while **C_{10}-TBBT-V** (IP: 5.4 eV) based TFT without F_4–TCNQ results in larger threshold voltages of −35 V (see Fig. S22, S23 and Table S5, ESI†). On the other hand, the lowly soluble **α-C_{10}-Th-TBBT-V** does not form a well-oriented crystal thin film, resulting in a low mobility of 0.55 $cm^2\ V^{-1}\ s^{-1}$ (Fig. S19, ESI†). Further studies on the optimization of the length of alkyl chains, resultant solubility, and crystallinity may elucidate the potential of the carrier transporting ability.

Table 3 OFET characteristics of **TBBT-V** derivatives

Compounds	μ^a ($cm^2\ V^{-1}\ s^{-1}$) μ_{max}	μ_{ave}	$V_{th}{}^b$ (V)	I_{on}/I_{off}
C_{10}-TBBT-V	6.2	4.6	−15 to −20	10^6
α-C_{10}-Th-TBBT-V	0.55	0.53	0 to −10	10^5
β-C_{10}-Th-TBBT-V	2.3	1.6	0 to −10	10^6

[a] Data from 6–10 good devices. Estimated from the saturation regime. [b] SiO_2 200 nm.

Conclusions

In summary, we focused on the **TBBT-V** core as an easily functionalized core as well as a moderately soluble platform. Employing brominated **TBBT-V** we synthesized decyl and alkyl thienyl moiety substituted derivatives. Although the **C_{10}-TBBT-V** adopts the aggregated form with a non-negligible displacement along the molecular long axis, the molecules achieve overlapping packing motifs in the crystal. Substitution of the alkylated thienyl moieties introduces an efficient extension of the π-conjugated system, resulting in a small ionization potential. Among the **TBBT-V** derivatives, **C_{10}-TBBT-V** and **β-C_{10}-Th-TBBT-V** exhibit high FET performances with mobilities as high as 6.2 and 2.3 $cm^2\ V^{-1}\ s^{-1}$ in their single crystalline thin films, respectively. Notably, **β-C_{10}-Th-TBBT-V** shows a negligible threshold voltage. Further systematic investigations of the substituents should lead to a higher performance by finely modulating the material-solubility as well as the packing geometry. Extensive exploration of **TBBT-V** derivatives and their congeners is now underway in our laboratory.

Experimental section

Materials: reagents and starting materials

2,3-Dibromothiophene, $NaCNBH_3$, 1-iododecane, 2,2,6,6-tetramethylpiperidine, 1,1,2,2-tetrachlorodibromoethane, tetrakis-triphenylphosphine palladium(0), [1,1′-bis(diphenylphosphino)-ferrocene]dichloropalladium(II) dichloromethane adduct, 3-decylthiophene, and trimethyltin chloride were purchased from TCI. 2,5-Thiophenedicarboxaldehyde, *n*-decylmagnesiumbromide, and zinc chloride were purchased from Sigma-Aldrich Inc. Zinc iodide was purchased from WAKO chemicals. 1.6 M *n*-BuLi in hexane, lithium chloride, and potassium phosphate were purchased from KANTO chemicals. All anhydrous solvents were purchased from KANTO chemicals. **TBBT-V**, 2-decylthiophene, 2-(trimethylstannyl)-4-decylthiophene, and 2-(trimethylstannyl)-5-decylthiophene were synthesized according to the literature.[12,19,20]

General methods for synthesis and characterization

All the reactions were carried out under an atmosphere of nitrogen. Air- or moisture-sensitive liquids and solutions were

transferred *via* a syringe or a Teflon cannula. Analytical thin-layer chromatography (TLC) was performed on glass plates with 0.25 mm 230–400 mesh silica gel containing a fluorescent indicator (Merck Silica gel 60 F254). TLC plates were visualized by exposing them to an ultraviolet lamp (254 nm and 365 nm), dipping with 10% phosphomolybdic acid in ethanol, and heating on a hot plate. Flash column chromatography was performed on Kanto silica gel 60. Open column chromatography was performed on Wakogel C-200 (75–150 μm). All NMR spectra were recorded on an ECS400 spectrometer. Chemical shifts were reported in parts per million (ppm, δ scale) from the residual protons in the deuterated solvent for ^{1}H NMR (δ 7.26 ppm for chloroform and δ 5.93 ppm for 1,1,2,2-tetrachloroethane) and from the solvent carbon for ^{13}C NMR (*e.g.*, δ 77.16 ppm for chloroform). The data were presented in the following format: chemical shift, multiplicity (s = singlet, d = doublet, t = triplet, m = multiplet), coupling constant in Hertz (Hz), the signal area integration in natural numbers, and assignment (italic). Mass spectra were measured on a JEOL JMS-T100LC APCI/ESI mass spectrometer. Melting points and elemental analyses were collected on a Mettler Toledo MP70 Melting Point System and a J-Science Lab JM10 MICRO CORDER, respectively. Photoelectron yield spectroscopy (PYS) was performed on a Sumitomo Heavy Industries Advanced Machinery PYS-202. For the PYS measurements, thin films (100 nm) were thermally evaporated on ITO coated quartz substrates and measurements were performed in a vacuum. UV-vis absorption spectra were measured with a JASCO V-570 spectrometer. Thin films (100 nm thick) were prepared by vacuum deposition on quartz substrates.

Synthesis

Preparation of lithium tetramethylpiperidide (LiTMP). To a solution of 2,2,6,6-tetramethylpiperidine (TMP) (46.6 mL, 274 mmol) in THF (274 mL) was added *n*-BuLi (1.60 M hexane solution, 171 mL, 274 mmol) at −78 °C. After stirring at 0 °C for 30 min, the LiTMP solution was obtained.

Synthesis of Br-TBBT-V. To a white suspension of **TBBT-V** (2.96 g, 10.0 mmol, 1.00 mol amt.) in THF (100 mL) was added LiTMP in solution (0.54 M in THF and hexane, 46.3 mL, 25.0 mmol, 2.50 mol amt.) using a Teflon cannula at −78 °C and stirred at that temperature for 2 h. To the resulting wine red suspension, 1,1,2,2-tetrachlorodibromoethane (9.77 g, 30.0 mmol, 3.00 mol amt.) in THF (30 mL) was added using a Teflon cannula at −98 °C. After stirring at −98 °C for 2 h, the reaction mixture was warmed to room temperature and stirred for 10 h. The resulting pale pink precipitate was collected by filtration, followed by recrystallization from 1,2-dichlorobenzene to afford the title compound (3.68 g, 8.10 mmol, 81%) as a white solid. m.p.: over 300 °C. ^{1}H NMR (400 MHz, $CDCl_2CDCl_2$, 100 °C): δ 7.44 (s, 2H, Ar*H*), 8.12 (s, 2H, Ar*H*), 8.44 (s, 2H, Ar*H*). ^{13}C NMR was not recorded due to the poor solubility. TOF MS (APCI+): Calcd for $C_{16}H_7Br_2S_3$ [M + H] 453, found, 453. Anal. Calcd for $C_{16}H_6Br_2S_3$: C, 42.31; H, 1.33. Found: C, 42.47; H, 1.20.

Synthesis of C_{10}-TBBT-V. To an *n*-decylmagnesium bromide solution (1.0 M in diethylether, 4.80 ml, 4.80 mmol), a zinc chloride solution (1.0 M in THF, 4.80 ml, 4.8 mmol) was added at 0 °C. To the organozinc reagent, **Br-TBBT-V** (545 mg, 1.20 mmol), [1,1′-bis(diphenylphosphino)ferrocene]dichloropalladium(II) dichloromethane adduct (49 mg, 0.06 mmol) and toluene (12 mL) were added and stirred at 70 °C for 18 h. An excess amount of MeOH was added, and the precipitate was collected by filtration. The precipitate was purified by recrystallization from 1,2-dichlorobenzene/hexane to afford the desired product (440 mg, 0.763 mmol, 64% yield) as a white solid. m.p.: 190.9–191.2 °C. ^{1}H NMR (400 MHz, $CDCl_2CDCl_2$) δ 0.82 (t, J = 6.4Hz, 6H, CH_3) 1.21–1.36 (m, 28H, CH_2), 1.72 (quin, J = 7.5 Hz, 4H, ArCH$_2$CH_2), 2.88 (t, J = 7.2 Hz, 4H, ArCH_2), 7.09 (s, 2H, Ar*H*), 8.11 (s, 2H, Ar*H*), 8.39 (s, 2H, Ar*H*). ^{13}C NMR (100 MHz, $CDCl_3$, 25 °C): δ 14.21, 22.78, 29.25, 29.42, 29.48, 29.65, 29.69, 31.09 (two overlapping carbons), 31.99, 114.66, 115.66, 120.23, 133.25, 135.52, 137.97, 138.94, 146.78. TOF HRMS (APCI+): Calcd for $C_{36}H_{49}S_3$ [M + H] 577.2996, found, 577.2983. Anal. Calcd for $C_{36}H_{48}S_3$: C, 74.94; H, 8.39. Found C, 74.80; H, 8.38.

Typical Stille coupling procedure to synthesize Th–TBBT–V derivatives: synthesis of β-C_{10}-Th-TBBT-V. To a suspension of 2-trimethylstannyl-4-*n*-decylthiophene (1.01 g, 2.60 mmol, 2.60 mol amt.) and **Br-TBBT-V** (454 mg, 1.00 mmol, 1.00 mol amt.) in DMF (10 mL) were added tetrakis(triphenylphosphine)-palladium(0), (57.8 mg, 0.05 mmol, 5.00 mol%) and LiCl (110 mg, 2.60 mmol, 2.60 mol amt.). The resulting mixture was heated to 100 °C and stirred for 10 h. After the reaction mixture was quenched by a 10% KF aqueous solution, the resulting precipitate was collected by filtration, and washed with DMF and acetone. The collected solid material was dissolved in hot 1,2-dichlorobenzene and passed through Celite and a short pad of a silica gel column to remove inorganic materials. After removing the solvent *in vacuo*, the desired product was obtained (682 mg, 0.921 mmol, 92% yield) as a pale yellow solid. m.p.: 198.3–198.7 °C. ^{1}H NMR (400 MHz, $CDCl_2CDCl_2$, 100 °C) δ 0.82 (t, J = 6.4 Hz, 6H, CH_3), 1.20–1.32 (m, 28H, (CH_2)$_7$), 1.60 (quin, J = 7.2 Hz, 4H, ArCH$_2$CH_2), 2.56 (t, J = 7.2 Hz, 4H, ArCH_2), 6.89 (s, 2H, Ar*H*), 7.12 (s, 2H, Ar*H*), 7.47 (s, 2H, Ar*H*), 8.14 (s, 2H, Ar*H*), 8.44 (s, 2H. Ar*H*). TOF HRMS (APCI+): Calcd for $C_{44}H_{53}S_5$ [M + H] 741.2751, found, 741.2723. Anal. Calcd for $C_{44}H_{52}S_5$: C, 71.30; H, 7.07. Found: C, 71.25; H, 7.14.

Synthesis of α-C_{10}-Th-TBBT-V. Yield: 87%. Pale yellow solid. m.p.: 261.4–261.9 °C. ^{1}H NMR (400 MHz, $CDCl_2CDCl_2$, 100 °C) δ 0.89 (t, J = 6.8 Hz, 6H, CH_3), 1.28–1.44 (m, 28H, (CH_2)$_7$), 1.73 (quin, J = 7.2 Hz, 4H, ArCH$_2$CH_2), 2.83 (t, J = 7.2 Hz, 4H, ArCH_2), 6.74 (d, J = 3.6 Hz, 2H, Ar*H*), 7.13 (d, J = 3.6 Hz, 2H, Ar*H*), 7.43 (s, 2H, Ar*H*), 8.14 (s, 2H, Ar*H*), 8.45 (s, 2H, Ar*H*). TOF HRMS (APCI+): Calcd for $C_{44}H_{53}S_5$ [M + H] 741.2751, found, 741.2723. Anal. Calcd for $C_{44}H_{52}S_5$: C, 71.30; H, 7.07. Found: C, 71.12; H, 7.04.

OFET device fabrication and evaluation procedure

Purification of materials for device fabrication. **C_{10}-TBBT-V**, **α-C_{10}-Th-TBBT-V**, and **β-C_{10}-Th-TBBT-V** were purified by crystallizing twice from either toluene or 1,2-dichlorobenzene and subliming twice to obtain pure materials.

Fabrication and evaluation of solution-crystallized single crystal devices. Powders of **C_{10}-TBBT-V**, **α-C_{10}-Th-TBBT-V**, and **β-C_{10}-Th-TBBT-V** were dissolved in anisole and 1,2-dichlorobenzene at a

hot plate temperature of approximately 40, 50, and 120 °C to a concentration of 0.05, 010, and 0.10 wt%, respectively. Semiconductor films were prepared from the solution by edge-casting.[15] All of the samples were prepared on Si/SiO_2 substrates treated with vapor-deposited β-PTS-SAMs. The whole setup was heated on a hot plate at the optimized temperature for each solution (approximately 60–70 °C), and the solution was poured into the edge of the sustaining piece. The semiconductor crystal grew as the solvent evaporated in the direction illustrated by the red arrows (Fig. 4a). The crystalline thin film was typically a few hundred nanometers thick. Onto the solution-crystallized film, gold electrodes (40 nm) as well as source and drain contacts were vacuum deposited through a shadow mask after depositing F_4–TCNQ (2 nm) to construct the device geometry of the top-contact configuration. Finally, to prevent misevaluation, the channels were shaped into a rectangle using a laser-etching technique so that L and W were properly identified. The typical length (L) of the channels was 100 μm. The doped-Si layer acted as the gate electrode, and SiO_2 behaved as a gate insulator with a relative dielectric constant of 3.9. The F_4–TCNQ layers between the organic semiconductor and metal contacts were deposited to reduce the extrinsic contact resistance.[21] Electrical characterization was performed using a semiconductor parameter analyzer (Keithley 4200) with two source-measurement units (SMUs). The field-effect mobility values (μ_{FET}) were estimated from the saturation regime using the following equation

$$I_D = (WC_i/2L)\mu_{FET}(V_G - V_{th})^2$$

where C_i is the capacitance of the gate insulator and V_{th} is the threshold voltage.

Acknowledgements

This work was supported by the JST PRESTO program ''Molecular Technology and Creation of New Functions'' and KAKENHI. C. M. thanks JSPS for a Grant-in-Aid for Young Scientists (B) (No. 25810118). M. Y. thanks JSPS for a Grant-in-Aid for Scientific Research (C) (No. 26410254) and the Kansai University Subsidy for Supporting Young Scholars, 2014. T. O. also thanks JSPS for a Grant-in-Aid for Scientific Research (B) (No. 25288091). This work was performed under the Cooperative Research Program of ''Network Joint Research Center for Materials and Devices''.

References

1 S. R. Forrest, *Nature*, 2004, **428**, 911.
2 H. E. Katz, *Chem. Mater.*, 2004, **16**, 4748.
3 Z. Bao and J. Locklin, *Organic Field-Effect Transistors*, CRC Press, Florida, 1st edn, 2007.
4 J. E. Anthony, *Chem. Rev.*, 2006, **106**, 5028.
5 K. Takimiya, S. Shinamura, I. Osaka and E. Miyazaki, *Adv. Mater.*, 2011, **23**, 4347.
6 Y. Y. Lin, D. J. Gundlach, S. F. Nelson and T. N. Jackson, *IEEE Electron Device Lett.*, 1997, **18**, 606.
7 T. Yamamoto and K. Takimiya, *J. Am. Chem. Soc.*, 2007, **129**, 2224.
8 M. J. Kang, I. Doi, H. Mori, E. Miyazaki, K. Takimiya, M. Ikeda and H. Kuwabara, *Adv. Mater.*, 2011, **23**, 1222.
9 K. Nakayama, Y. Hirose, J. Soeda, M. Yoshizumi, T. Uemura, M. Uno, W. Li, M. J. Kang, M. Yamagishi, Y. Okada, E. Miyazaki, Y. Nakazawa, A. Nakao, K. Takimiya and J. Takeya, *Adv. Mater.*, 2011, **23**, 1626.
10 H. Ebata, T. Izawa, E. Miyazaki, K. Takimiya, M. Ikeda, H. Kuwabara and T. Yui, *J. Am. Chem. Soc.*, 2007, **129**, 15732.
11 T. Okamoto, C. Mitsui, M. Yamagishi, K. Nakahara, J. Soeda, Y. Hirose, K. Miwa, H. Sato, A. Yamano, T. Matsushita, T. Uemura and J. Takeya, *Adv. Mater.*, 2013, **25**, 6392.
12 B. Wex, B. R. Kaafarani and D. C. Neckers, *J. Org. Chem.*, 2004, **69**, 2197.
13 B. Wex, B. R. Kaafarani, R. Schroeder, L. A. Majewski, P. Burckel, M. Grell and D. C. Neckers, *J. Mater. Chem.*, 2006, **16**, 1121.
14 B. Wex, F. M. Jradi, D. Patra and B. R. Kaafarani, *Tetrahedron*, 2010, **66**, 8778.
15 T. Uemura, Y. Hirose, M. Uno, K. Takimiya and J. Takeya, *Appl. Phys. Express*, 2009, **2**, 111501.
16 L. Pauling, *The Nature of the Chemical Bond*, Cornell University Press, 3rd edn, 1960.
17 E. F. Valeev, V. Coropceanu, D. A. da Silva Filho, S. Salman and J.-L. Brédas, *J. Am. Chem. Soc.*, 2006, **128**, 9882.
18 M. C. R. Delgado, E.-G. Kim, D. A. d. S. Filho and J.-L. Bredas, *J. Am. Chem. Soc.*, 2010, **132**, 3375.
19 T. Bjørnholm, D. R. Greve, N. Reitzel, T. Hassenkam, K. Kjaer, P. B. Howes, N. B. Larsen, J. Bøgelund, M. Jayaraman, P. C. Ewbank and R. D. McCullough, *J. Am. Chem. Soc.*, 1998, **120**, 7643.
20 A. J. J. M. van Breemen, P. T. Herwig, C. H. T. Chlon, J. Sweelssen, H. F. M. Schoo, S. Setayesh, W. M. Hardeman, C. A. Martin, D. M. de Leeuw, J. J. P. Valeton, C. W. M. Bastiaansen, D. J. Broer, A. R. Popa-Merticaru and S. C. J. Meskers, *J. Am. Chem. Soc.*, 2006, **128**, 2336.
21 T. Minari, T. Miyadera, K. Tsukagoshi, Y. Aoyagi and H. Ito, *Appl. Phys. Lett.*, 2007, **91**, 05350.